EJGE

An Algorithm for the Propagation of Uncertainty in Soils using the Discrete Element Method

Viet D.H. Tran

Viet D.H. Tran, Graduate student
Department of Civil Engineering and Applied Mechanics, McGill University.
e-mail: viet.tran@mail.mcgill.ca

Mohamed A. Meguid

Associate Professor (Corresponding Author)
Department of Civil Engineering and Applied Mechanics, McGill University.
Tel. (514) 398-1537 - Fax. (514) 398-7361, e-mail: mohamed.meguid@mcgill.ca

Luc E. Chouinard

Luc E. Chouinard, Associate Professor
Department of Civil Engineering and Applied Mechanics, McGill University.
Tel. (514) 398-6446 - Fax. (514) 398-7361
e-mail: luc.chouinard@mcgill.ca

ABSTRACT

An efficient algorithm to create discrete element samples with predefined properties incorporating the random field theory is introduced in this paper. The algorithm considerably reduces the time needed to generate a large scale domain as only a small initial sample with dynamic packing is used. Three-dimensional anisotropic random fields are generated using the Local Average Subdivision (*LAS*) method accounting for the spatial variability. The random fields are then mapped on the discrete element domain and uncertain parameters of each particle are obtained from the corresponding random field cell. Triaxial tests are conducted on large soil samples with the dimensions of 1.5m x 3.0m x 1.5m comprising over 150,000 spherical particles. The microscopic friction angle and stiffnesses of the particles are selected as random variables since they have a significant effect on the soil behavior under triaxial testing conditions. Monte Carlo simulation is implemented to analyze the probabilistic features of the output values.

KEYWORDS: Discrete element method; Packing algorithm; Random field; Spatial variability

INTRODUCTION

Reliability analysis of geotechnical structures has been traditionally performed using the First-Order Second Moment method (FOSM), the First-Order Reliability Method (FORM), the Point Estimate Method (PEM) and Monte-Carlo simulation (Christian et al., 1994; Christian and Baecher, 1999; Baecher and Christian, 2003; Low et al., 2011). While FORM and FOSM are based on approximate assumptions related to the derivation of the performance function, these two methods may not be suitable for nonlinear

problems. Although the PEM is being widely used in geotechnical engineering, there are some limitations regarding its simplicity (Baecher and Christian, 2003). Recent developments in numerical methods have made it more feasible to combine reliability analyses with numerical simulations. Schweiger et al. (2001) proposed a framework that employs the deterministic finite element method in reliability analyses. In this approach, the PEM was used in conjunction with the Finite Element Method to analyze the probabilistic behavior of a sheet-pile wall and tunnel excavation process. Although this approach accounts for variability of soil properties in the deterministic finite element method, it does not consider the spatial variability of soil properties. Schweiger and Peschl (2005) used the Random Set Finite Element Method to take into account the spatial correlation in an approximate way. However, spatial variation can be better represented by random field theory. The Random Finite Element Method (RFEM) which combines random field theory and Monte-Carlo simulation has been successfully used for several geotechnical engineering problems such as bearing capacity (Suchomel and Mašin, 2010), settlement (Fenton and Griffiths, 2005; Griffiths and Fenton, 2009) , pillar stability (Griffiths et al., 2002), steady seepage (Griffiths and Fenton; 1998) and slope stability (Griffiths and Fenton; 2004).

An alternative numerical method that can be used for geotechnical problems is the Discrete Element Method (DEM). The method proposed by Cundall and Strack (1979) has proven to be a versatile approach for the simulation of granular materials. A DEM model is usually built using a set of particles interacting at contact points, making it possible to describe the behavior of granular soils under large deformations. This method has also been implemented to solve geotechnical applications including pile driving (Lobo Guerrero and Vallejo, 2005), tunnel excavation (Melis Maynar and Medina Rodriguez, 2005) and rockfill dam (Deluzarche and Cambou, 2006).

Suchomel and Mašin (2010) suggested that random field theory can be combined with the DEM. The method, however, has hardly been applied in conjunction with reliability analysis partly due to the large computational time required and the limitation of computer capacity. Hsu and Nelson (2006) used the same approach for the slope stability analysis of weak rock masses. The spatial variability of material properties was considered with random field elements embedded in the numerical analyses. The rock mass was simulated using two-dimensional (2D) discrete elements with a maximum of 10 different material properties available in the UDEC program. This limitation did not allow for a proper representation of the spatial variability of material properties.

There are several issues that have to be considered when implementing reliability analysis with the DEM: (1) spatial variability has to be considered in the discrete element model to represent real condition, (2) the total computational time required for the packing process of a large-scale model should be acceptable, and (3) the random field of material properties has to be mapped onto the discrete element domain defined by the packing algorithm. This paper presents an algorithm that satisfies these criteria.

In this study, the packing algorithm suggested by Dang and Meguid (2010) is adopted since it allows for the generation of 3D packing models with pre-defined properties and the time required to create large-scale domains is reduced considerably. The particle domain obtained with this technique is meshed into a user-defined 3D grid to which the anisotropic random fields are assigned using the Local Average Subdivision method proposed by Fenton and Vanmarcke (1990). Triaxial test simulations are performed to demonstrate the effect of material variability on the behavior of soil samples.

GENERATION OF THE PARTICLE DOMAIN

Packing algorithm

The packing procedure consists of two phases: in phase 1, a relatively small size initial packing is

first generated with a predefined grain size distribution and a target porosity. The final packing is then generated in phase 2 by assembling the small samples using the "flip technique" to maintain the same grain size distribution and porosity (Dang and Meguid, 2010).

The details of each phase are as follow:

Phase 1: The dimensions of a box for the initial packing are denoted in the x, y and z directions as (b_x x b_y x b_z). A number of non-overlapping particles are then generated inside the box with the dimensions of (b_x x h_y x b_z) where the height h_y of the box is larger than b_y to ensure that all particles can settle under gravity into the box. Additional particles are generated until the target volume of all particles is reached:

$$V_s = p.b_x.b_y.b_z \tag{1}$$

where V_s is the target volume of particles and p is the target porosity of the packing.

In order to obtain the initial packing with a predefined particle size distribution, the radius of a particle i is randomly generated from the grain size distribution (Fu and Dekelbab, 2003):

$$r_i = [D_1 + (RAN_i \times 100 - P_1) \times \frac{(D_2 - D_1)}{(P_2 - P_1)}]/2 \tag{2}$$

where r_i is the radius of particle i, RAN_i is a uniformly distributed random number generated in the range $0 \leq RAN_i < 1$, P_1 and P_2 are the percentage of grains (%) passing through sieves S_1 and S_2 such that $P_1 \leq 100.RAN_i < P_2$, sieve S_1 and S_2 are then specified by P_1 and P_2, D_1 and D_2 are the diameters of sieves S_1 and S_2. After the packing reaches the stability condition, it is still a loose structure. A compaction procedure with a combination of shaking and vertical compression is applied in order to obtain the target porosity. Phase 1 continues until the initial packing satisfies the stability condition.

Phase 2: The "flip technique" is implemented in this phase to overcome the large amount of computations associated with the dynamic packing method. The technique is a 3D process and is illustrated in Fig. 1.

The final packing space with the dimensions of (p_x x p_y x p_z) is divided into (n_x x n_y x n_z) domains. An initial packing S_0 (b_x x b_y x b_z) generated using the technique described in phase 1 is cloned repeatedly to obtain a final packing with similar properties. All particles which were initially in contact with the walls now become in contact with other particles in the final packing.

The initial packing S_0 is first placed into the lower left corner of the domain. Block S_{yz}, obtained by flipping S_0 around the y-z plane, is placed to the right of sample S_0. A second sample S_0 is then placed to the right of S_{yz} and the process is repeated until the first row is completed. The entire first row is then flipped around the x-z plane in a similar process to obtain the second row, and the process is repeated to generate the first slice consisting of (n_x x n_y) small blocks in n_x columns and n_y rows. The first slice is flipped around the x-y plane to generate the second slice, and the final packing is obtained by repeating the process. Finally, the final packing is allowed to reach the stability condition.

In order to identify the position of a particle in the soil sample grid, each particle is marked by the block from which it is generated. A block that is of slice k, row j and column i within that row is noted as (i, j, k); all spheres of that block are then identified by (i, j, k).

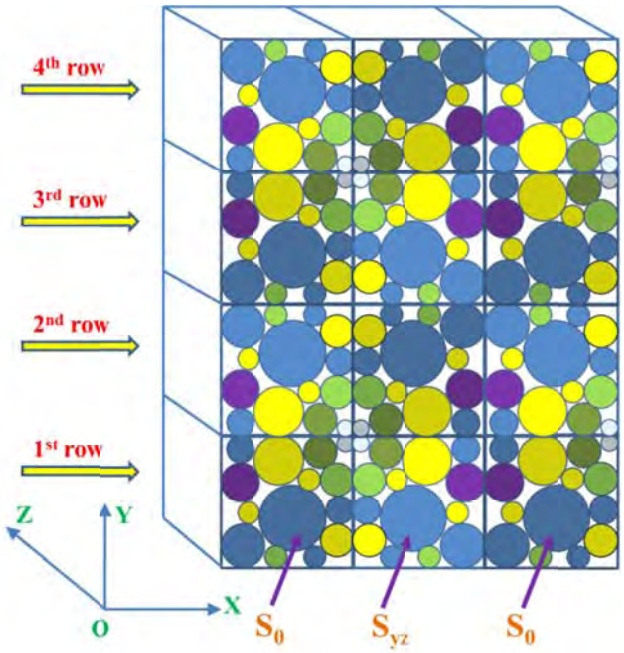

Figure 1: Flip technique to obtain the final packing

Packing process

The above packing algorithm is used to generate a soil sample, which has the dimensions of 1.5m width, 3.0m height and 1.5m depth. The soil mass is formed from 6 x 12 x 6 = 432 small initial blocks, each block is cubic with the dimensions of 0.25m x 0.25m x 0.25m.

A simple contact law is applied in this study to calculate contact forces. The force vector $\vec{\mathbf{F}}$ which represents the interaction between two particles is decomposed into normal and tangential forces:

$$\vec{\mathbf{F}}_n = K_n.\vec{\mathbf{\Delta}}_n\,,\ \ \delta\vec{\mathbf{F}}_s = -K_s.\delta\vec{\mathbf{\Delta}}_s \qquad (3a, b)$$

where $\vec{\mathbf{F}}_n$ and $\vec{\mathbf{F}}_s$ are the normal and tangential forces; K_n and K_s are the normal and tangential stiffnesses at the contact; $\delta\vec{\mathbf{\Delta}}_s$ is the incremental tangential displacement and $\vec{\mathbf{\Delta}}_n$ is the normal penetration between the two particles.

K_n and K_s are defined by the following equations:

$$K_n = r\frac{k_n^A.k_n^B}{k_n^A + k_n^B} \qquad K_s = r\frac{k_s^A.k_s^B}{k_s^A + k_s^B} \qquad (4a, b)$$

where k_n and k_s are the normal and tangential stiffnesses of two contact particles A and B, respectively; r is the average radius calculated by:

$$r = \frac{r_A + r_B}{2} \qquad (5)$$

The shear process is activated when the following condition is satisfied:

$$F_s \geq F_n . \tan(\phi) \quad (6)$$

where ϕ is the internal friction angle.

The particles are assumed to have properties of granular material with no cohesion. The target porosity of the sample is 0.40. The target grain size distribution is given in Table 1 and the material properties of the particles during the packing process are given in Table 2.

Table 1: Grain size distribution

Sieve diameter (mm)	% passing
10	0
20	0
40	31.47
100	90.93
160	99.64
200	100

Table 2: Material properties for the packing process

Parameter	Value
Particle density (kg/m^3)	2600
Particle normal stiffness k_n (Pa)	9 x 10^8
Ratio k_s/k_n	0.1
Friction angle ϕ (radians)	0.6
Box's Poisson's ratio	0.2
Box's friction (degrees)	0
Force damping coefficient	0.2
Moment damping coefficient	0.2

RANDOM FIELD GENERATOR

Soil properties at each location within the soil mass are considered to be random variables and typically exhibit considerable variation from point to point. Therefore, it is essential to consider the spatial variability of the soil domain. Neglecting the spatial variability may lead to the underestimation or overestimation of the probability of unsatisfactory performance (Griffiths and Fenton, 2004).

Several approaches have been proposed to generate spatially varying random fields including the Turning Bands Method, the Cholesky decomposition technique and the Local Average Subdivision Method (LAS) (Baecher and Christian, 2003). The LAS method has been chosen in this study as it allows for the implementation in numerical methods. In addition, it generates a discrete grid of local averages of a standard Gaussian random field and represents a random field accurately even for coarse meshes (Matthies et al., 1997).

In this study, the microscopic friction angle and the stiffnesses of particles are assumed to be random variables as they have a great influence on the behavior of soil samples (Belheine et al., 2009). The friction angle and stiffness are assumed to be uncorrelated and their spatial variability is examined

separately.

The friction angle ϕ, which is bounded both above and below, is assumed to follow a bounded distribution (Fenton and Griffiths, 2003):

$$\phi(\tilde{x}_i) = \phi_{\min} + \frac{1}{2}(\phi_{\max} - \phi_{\min})\left[1 + \tanh\left(\frac{sG_{\phi}(\tilde{x}_i)}{2\pi}\right)\right] \quad (7)$$

where $\tilde{x}_i$ is the spatial position, $\phi_{\min}$ and $\phi_{\max}$ are the minimum and maximum microscopic friction angles, s is a factor determining the variability of the friction angle and $G(\tilde{x}_i)$ is a normally distributed random field with zero mean, unit variance and given correlation lengths. It is noted that the bounded distribution is symmetric and the mean is the midpoint between $\phi_{\min}$ and $\phi_{\max}$.

The normal and tangential stiffnesses are assumed to follow lognormal distributions. Since the cross correlation between k_n and k_s is usually not well known, the two stiffnesses are assumed to be perfectly correlated for the sake of simplicity. This assumption is appropriate for assemblies involving spherical particles (Antony et al., 2006). The ratio k_s/k_n is kept constant for all particles, which means only the random field of k_n is initially generated by the random field generator and the random field of k_s is obtained directly from k_n.

The distribution of k_n is characterized by the mean μ_{k_n}, the standard deviation σ_{k_n} and the correlation lengths. A log-normally distributed random field of k_n is given by:

$$k_n(\tilde{x}_i) = \exp\{\mu_{\ln k_n} + \sigma_{\ln k_n} G_{\ln k_n}(\tilde{x}_i)\} \quad (8)$$

The two parameters $\mu_{\ln k_n}$ and $\sigma_{\ln k_n}$ are obtained from the lognormal distribution transformations:

$$\sigma^2_{\ln k_n} = \ln(1 + COV^2_{k_n}), \ \mu_{\ln k_n} = \ln \mu_{k_n} - \frac{1}{2}\sigma^2_{\ln k_n} \quad (9a, b)$$

where COV_{k_n} is the coefficient of variation of k_n.

The random field $G(\tilde{x}_i)$ is generated using the 3-D Markovian correlation function:

$$\rho = \exp\left(-\sqrt{\left(\frac{2\tau_x}{\theta(x)}\right)^2 + \left(\frac{2\tau_y}{\theta(y)}\right)^2 + \left(\frac{2\tau_z}{\theta(z)}\right)^2}\right) \quad (10)$$

where τ_x, τ_y and τ_z are the three components of the distance between two points in the random field; $\theta(x)$, $\theta(y)$ and $\theta(z)$ are the correlation lengths in x, y and z direction. These correlation lengths account for the anisotropic character of the random field and represent the distance over which the spatially random variables tend to have significant correlation.

The horizontal correlation length is chosen greater than the vertical due to the fact that soil generated from a deposition process has strong variability in the vertical direction. This is referred to as anisotropic heterogeneity. It should be noted that the spatial correlation structure of soil domains, especially in the horizontal direction is usually not well known and requires a large amount of site exploration which is not always feasible. Therefore, the vertical correlation length is varied in this study from 0.01 m (much smaller than the soil sample size) to 10.0 m (larger than the soil sample size) and the horizontal correlation length is kept 10 times greater than the vertical. A plot of Markovian correlation function

which indicates the correlation between two points separated by $\tau_x = \tau_y = \tau_z$ is given in Fig. 2.

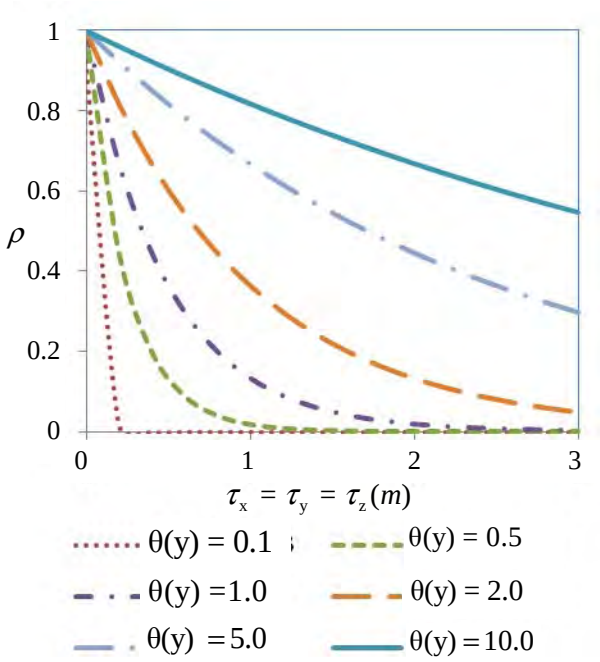

Figure 2: Markovian correlation function

In this study, ϕ_{min} and ϕ_{max} are determined to be 0.3 and 0.9 radians respectively, s is defined a value of 2.0, the value of COV_{k_n} is ranged from 0.4 to 2.0 while the mean value is kept constant as shown in Table 3.

In order to assign different realizations of the random field to the discrete element grid, the random field grid is made identical to the grid of the soil sample. Each random field is composed of 6 x 12 x 6 cells in the x, y and z direction, respectively. The dimensions of each cell are 0.25m x 0.25m x 0.25m, which are the same size as the initial packing of the sample.

Table 3: Probabilistic description for the random variables

Description	Parameter	Value
Stiffnesses	Mean μ_{k_n} (Pa)	9 x 10^8
	COV_{k_n}	0.4, 0.8, 1.2, 1.6, 2.0
	Ratio k_s/k_n	0.1
Friction angle	ϕ_{min} and ϕ_{max}	0.3 and 0.9
	S	2.0
Correlation lengths	$\theta(y)$ (m)	0.01, 0.1, 0.5, 1.0, 10.0
	$\theta(x)=\theta(z)$ (m)	0.1, 1.0, 5.0, 10.0, 100.0

NUMERICAL SIMULATION

Both the packing algorithm and the random field generator were implemented inside the open source code YADE (Kozicki and Donze, 2009; Šmilauer et al. 2010) to generate random soil samples. Since the random generation of particles is used in the packing procedure, the final assembly is obtained by executing the packing procedure only once using deterministic particle values to maintain the structure of the final packing.

In the first phase of the packing process, an initial packing that consists of 351 particles is generated. The expected grain size distribution of the packing is also achieved using Eq. (2). The final packing comprises 151,632 particles at the end of the second phase of the packing procedure and the properties of the initial packing are preserved through the flipping and cloning process. It can be seen from Fig. 3b that the vertical and horizontal stresses in the sample are consistent with the theoretical solutions ($\sigma_v=\sigma_{gz}$, $\sigma_h=\sigma_{gz}.K_0$).

Note that the dynamic packing procedure is applied only for the initial sample, and therefore, the total simulation time is greatly reduced. The entire packing process which requires nearly 72 hours using a personal computer is rather efficient compared to the time that would be required for packing a similar sample with over 150,000 particles.

The random field generator is then activated to generate several hundred sets of random fields for the random variables which are mapped on the final sample created by the packing process. Note that each sphere in the soil sample is marked by its identification generated from phase 2 of the packing procedure and the grid of the random field is identical to the grid of the soil sample, making it possible to connect the sphere with its corresponding random cell. Particles that are created in the same block are assigned the same values of the friction angle and stiffness.

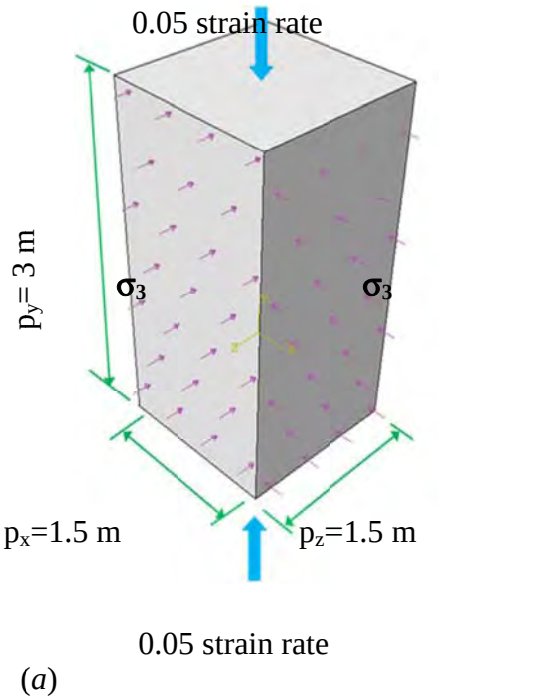

(*a*)

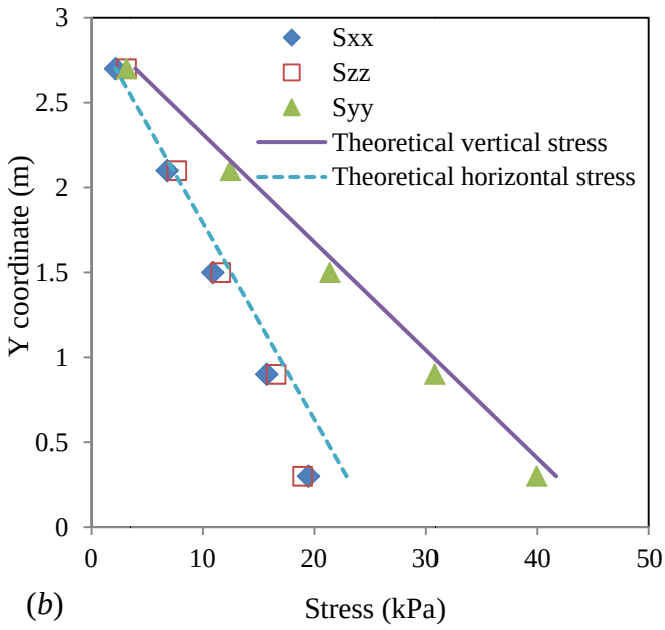

(*b*)

Figure 3: (*a*) Soil sample configuration. (*b*) The stress distribution in the sample

Fig. 4a and 4b show two typical random soil samples (with spatially varying stiffnesses) corresponding to $\theta_{\ln k_n}(y) = 1\,m$ and $\theta_{\ln k_n}(y) = 0.1\,m$ respectively. Lighter shaded regions indicate smaller k_n while darker shaded regions indicate larger k_n. The effect of the correlation lengths is also

evident: the smaller correlation lengths of the sample in Fig. 4b leads to larger spatial variation of k_n compared to the sample in Fig. 4a. In both cases, the larger horizontal correlation length results in more uniform k_n in the horizontal direction compared to the vertical direction.

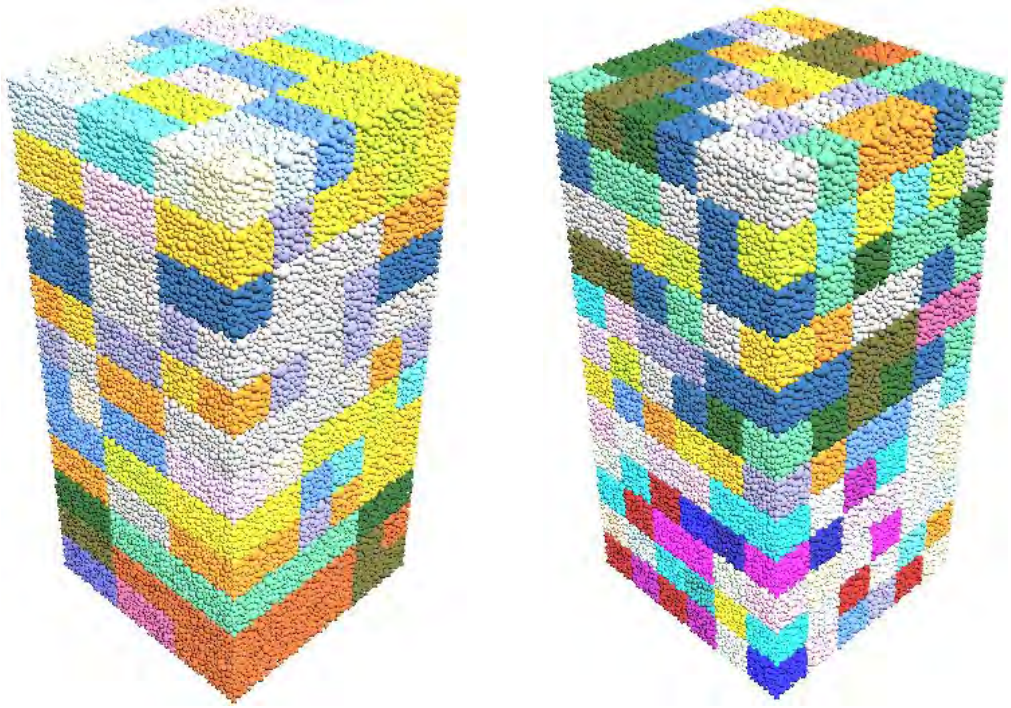

(*a*) (*b*)

Figure 4: Example of typical realizations

(*a*) $COV_{k_n} = 0.8$, $\theta(x) = \theta(z) = 10.0\text{m}$, $\theta(y) = 1.0\text{m}$

(*b*) $COV_{k_n} = 0.8$, $\theta(x) = \theta(z) = 1.0\text{m}$, $\theta(y) = 0.1\text{m}$

The effects of the variability of material properties are analyzed using Monte Carlo simulation. Numerical triaxial tests are performed on the randomly generated soil samples to analyze the probabilistic properties of the response. In each triaxial test, the sample is first compressed isotropically under a specified confining pressure. After the stability condition is reached, an additional strain rate of 0.1 is applied to the top surface while the pressures on the side walls are kept constant. Two different confining stresses of 100 kPa and 200 kPa are used in the analysis. The modulus E_{50} of the sample is obtained from the axial strain - deviator stress relationship at 50% of the maximum deviator stress and the macroscopic friction angle φ is obtained from the slope of the failure envelope based on Mohr-Coulomb failure criterion. Results of a typical test are illustrated in Fig. 5. It can be seen that, since there is no cohesion, the macroscopic failure envelope goes through the origin.

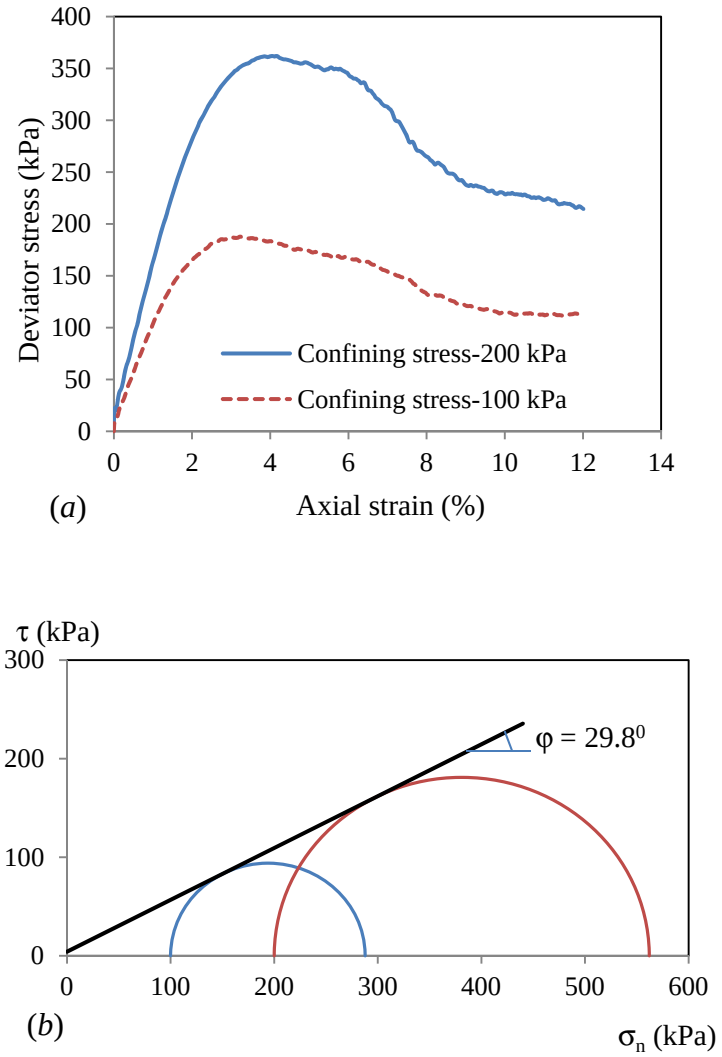

Figure 5: A typical triaxial test result
(*a*) Deviator stress versus axial strain curve. (*b*) Mohr circle presentation at peak strength

For each case of analysis, Monte Carlo simulations were performed for 250 realizations of random fields followed by the discrete element analysis of triaxial tests. Note that the number of realizations is limited by the execution time required for a single run (a numerical triaxial test requires about 5 hours on a personal computer with Core i7 Processor 2.8 GHz). To examine the stability of the Monte Carlo simulation, the mean value and standard deviation of E_{50} in accordance with the spatial variability of the stiffness are shown in Fig. 6 as a function of the cumulative number of simulation runs. The figure shows that the mean and standard deviation are quite stable for the sample size of 250.

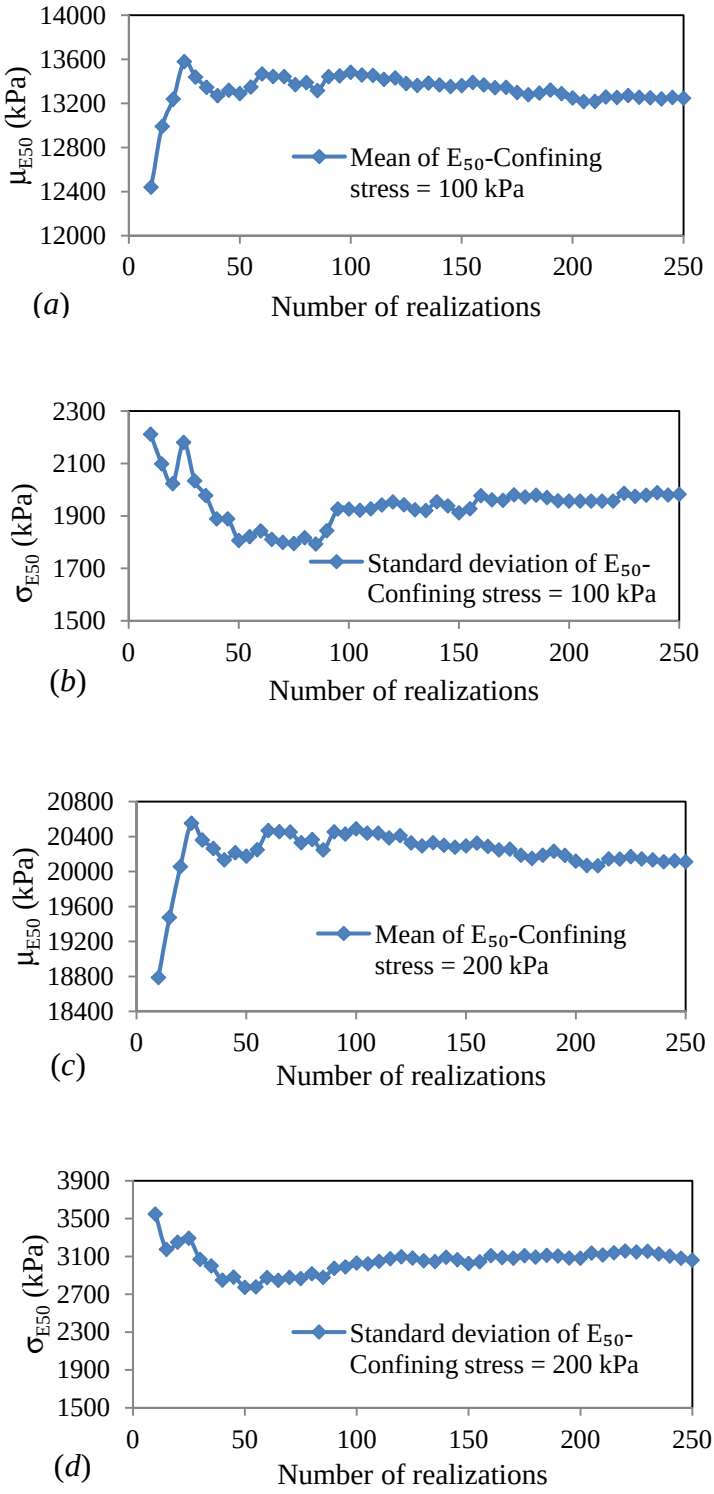

Figure 6: Mean and standard deviation of modulus E_{50} (case B - $COV_{k_n} = 0.8$, $\theta(y) = 1.0m$)

PROBABILISTIC ANALYSES

Two cases of the spatial variability including the microscopic friction angle and the stiffnesses are analyzed. For each case, only the analyzed random variable is varied while other parameters are kept constant as deterministic values.

Case A - Spatial variability of the friction angle

The histograms of the peak deviator stress $\Delta\sigma_f$ and macroscopic modulus E_{50} at a confining stress of 100 kPa in accordance with the spatial variability of the microscopic friction angle ϕ are shown in Fig. 7a and 7b. The fitting of the lognormal distributions is given in each histogram. It can be seen that although the microscopic friction angle follows a symmetric bounded distribution, the histograms of both the peak deviator stress and modulus E_{50} do not show a symmetric distribution. The lognormal distribution indicates the best fit with the histograms. The P-P plots for lognormal distribution fitting are presented in Fig. 8a and 8b.

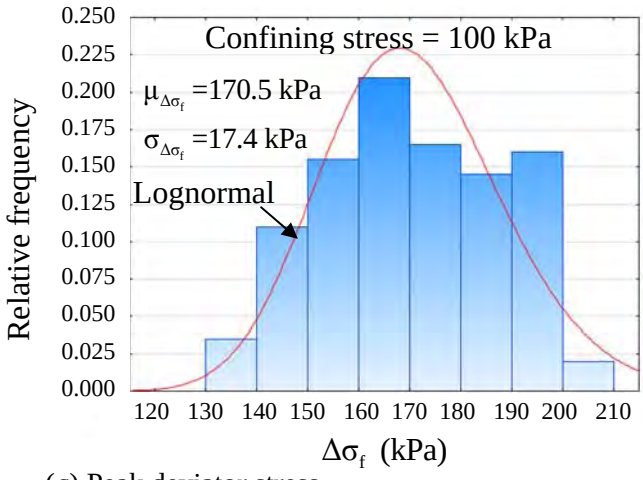

(*a*) Peak deviator stress

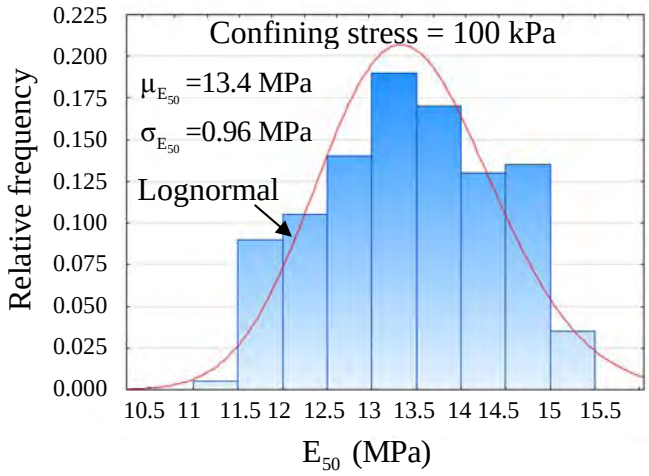

(*b*) Modulus

Figure 7: Histograms of macroscopic parameters (case A - $\theta(y) = 1.0\text{m}$)

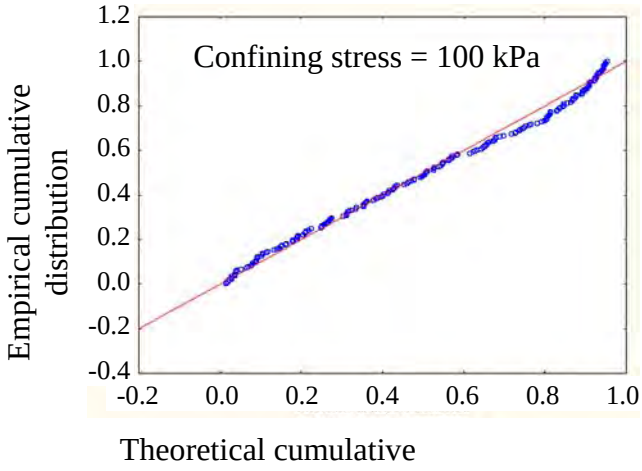

(*a*) Peak deviator stress

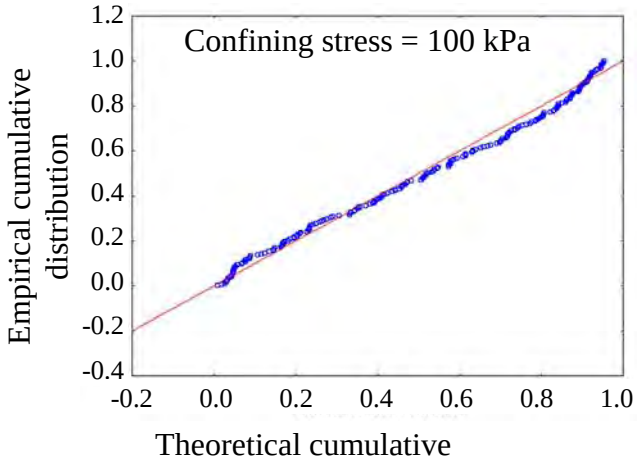

(*b*) Modulus E_{50}

Figure 8: P-P plots for lognormal distribution fitting (case A - $\theta(y) = 1.0m$)

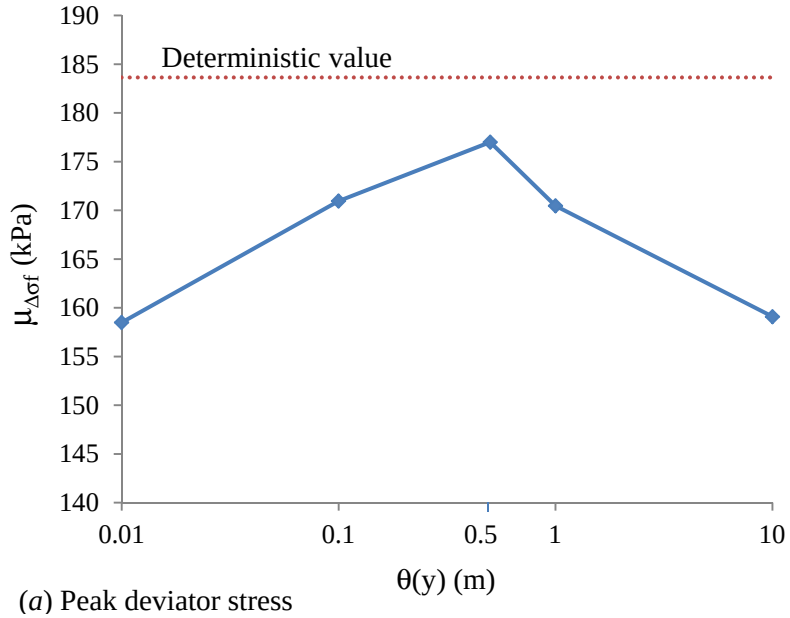

(*a*) Peak deviator stress

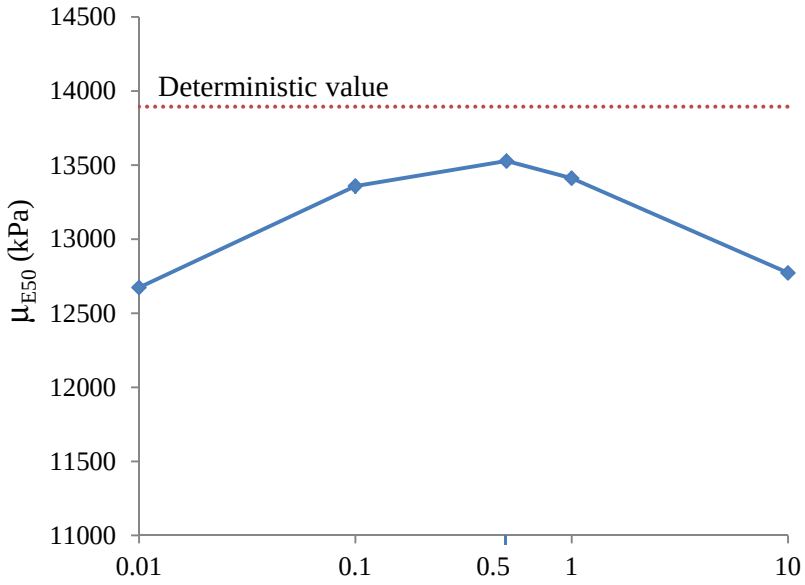

(*b*) Modulus E_{50}

Figure 9: Variation of $\mu_{\Delta\sigma_f}$ and $\mu_{E_{50}}$ (case A)

Fig. 9a and 9b show the variation of the mean values of the peak deviator stress ($\mu_{\Delta\sigma_f}$) and modulus ($\mu_{E_{50}}$) with different correlation lengths $\theta(y)$. It can be seen that the mean values of $\Delta\sigma_f$ and E_{50} are smaller than their deterministic values for all considered correlation lengths. For both high and low

correlation lengths, the mean values tend to their limits. Both $\mu_{\Delta\sigma_f}$ and $\mu_{E_{50}}$ have their maximum values at a vertical correlation length of about 0.5 m. It can be hypothesized that this correlation length results in a "rough" soil domain with high values of $\Delta\sigma_f$ and E_{50} while larger or smaller correlation lengths lead to smaller values. On the other hand, the standard deviations of the peak deviator stress ($\sigma_{E_{50}}$) and modulus ($\sigma_{\Delta\sigma_f}$) indicate an increase with the increase of $\theta(y)$ (see Fig.10a and 10b). When $\theta(y) \to 0$, the variances of $\Delta\sigma_f$ and E_{50} tend to zero since the local averaging results in a constant value for each simulation. No local averaging occurs when $\theta(y) \to \infty$ which results in high $\sigma_{E_{50}}$ and $\sigma_{\Delta\sigma_f}$.

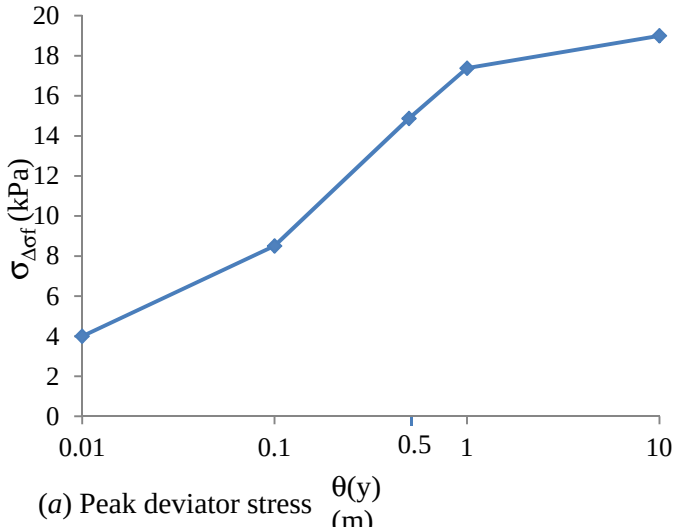

(*a*) Peak deviator stress

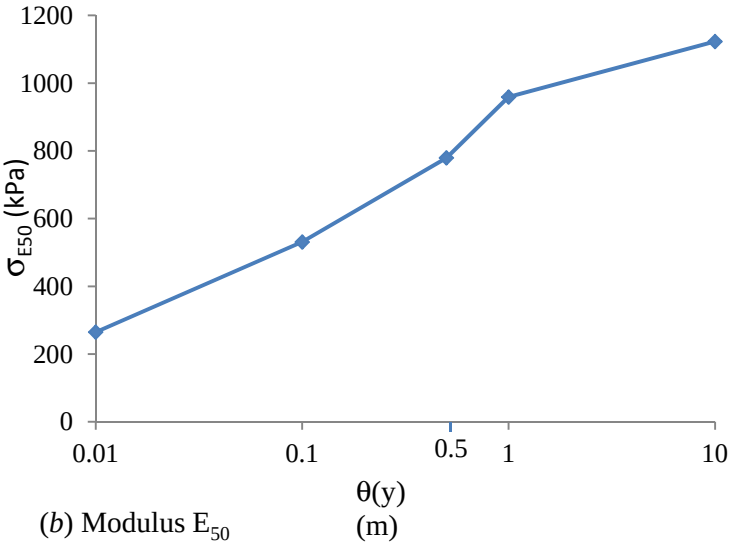

(*b*) Modulus E_{50}

Figure 10: Variation of $\sigma_{E_{50}}$ and $\sigma_{\Delta\sigma_f}$ (case A)

Case B - Spatial variability of the stiffness

It is observed that the spatial variability of the microscopic stiffness does not lead to a considerable variation of the peak deviator stress and therefore, only the modulus E_{50} is analyzed for this case. Histograms of E_{50} at two confining stresses are shown in Fig. 11. The shape of the histograms suggests a lognormal distribution. The fitted lognormal distribution, with parameters defined by the mean $\mu_{E_{50}}$ and the standard deviation $\sigma_{E_{50}}$, is given in each histogram. A statistical analysis indicates a good fit when a lognormal distribution is assumed. Both the Chi-Square goodness-of-fit test and the P-P plots demonstrate that the lognormal distribution is a good choice for the modulus E50 (Fig. 12). This is to be expected since the input random parameters kn and ks are log-normally distributed.

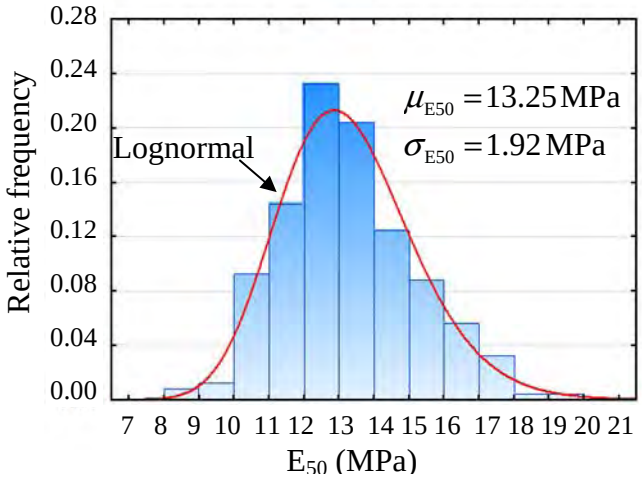

(*a*) Confining stress = 100 kPa

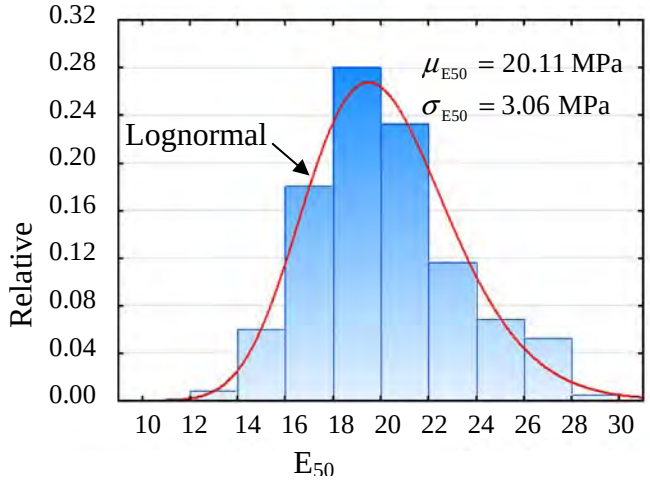

(*b*) Confining stress = 200 kPa

Figure 11: Histograms of modulus E_{50} (case B - $COV_{k_n} = 0.8$, $\theta(y) = 1.0m$)

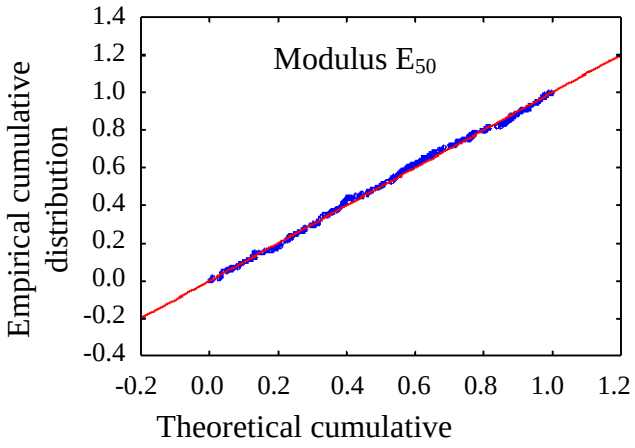

a) Confining stress = 100

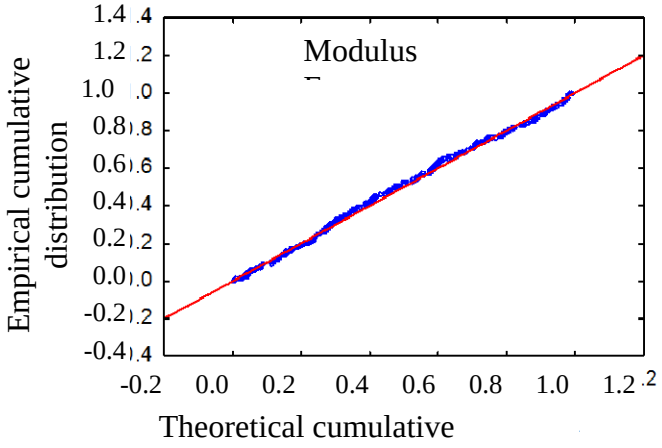

b) Confining stress = 200 kPa

Figure 12: Probability – Probability (P-P) plots for lognormal distribution fitting (case B - $COV_{k_n} = 0.8, \theta(y) = 1.0m$)

As shown in Fig. 13, the mean of E_{50} tends to a deterministic value for low values of the coefficient of variation COV_{k_n}. When COV_{k_n} tends to zero, E_{50} tends to the deterministic modulus which is obtained using the mean value of k_n for all particles in the sample domain. As COV_{k_n} increases, it is noted that $\mu_{E_{50}}$ decreases for all correlation lengths. This reduction implies that the macroscopic modulus is smaller than the deterministic modulus when spatial variability of soil properties is considered.

Fig. 13 also indicates that for both high and low correlation lengths, the mean value of E50 tends to its two limits. The maximum value of $\mu_{E_{50}}$ is obtained at an intermediate correlation length $\theta(y)$ of about 0.5 m. This observation is similar to the case of the spatial variability of the friction angle.

Fig. 14 illustrates the variation of the standard deviation of E_{50} as a function of COV_{k_n} and $\theta(y)$. It can be observed that $\sigma_{E_{50}}$ increases with the rise of COV_{k_n} and $\theta(y)$, and the largest value is reached when $\theta(y) \to \infty$. Due to the local averaging, $\sigma_{E_{50}}$ decreases when the correlation lengths are reduced.

From the spatial variability of the microscopic friction angle and stiffness, it can be seen that the mean values of the peak deviator stress and modulus are always smaller than their deterministic values while the standard deviations show an increase with the increase of the correlation length.

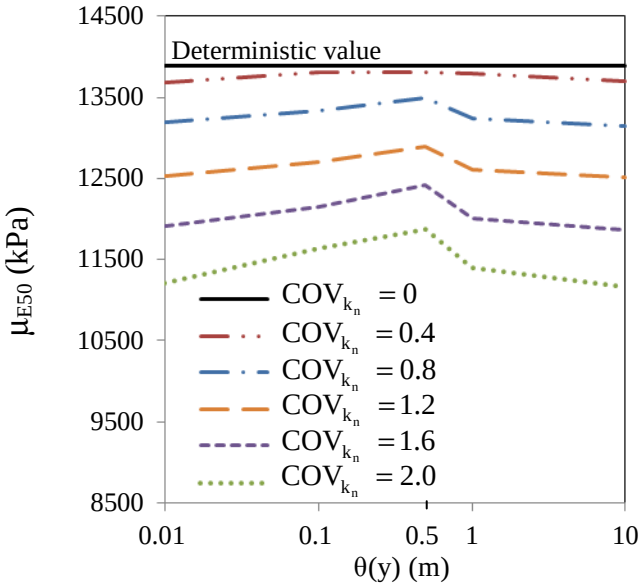

Figure 13: Variation of $\mu_{E_{50}}$ (case B)

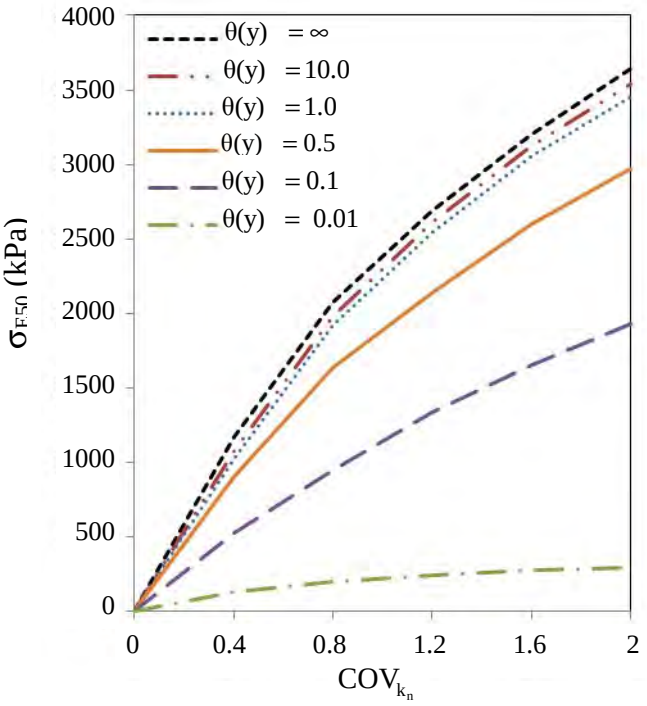

Figure 14: Variation of $\sigma_{E_{50}}$ (case B)

SUMMARY AND CONCLUSIONS

In this study, a framework to combine random field theories and the discrete element method to analyze the behavior of soil structures under spatially varying properties was presented. A triaxial testing of spatially varying soil samples was performed. Two confining stresses were used for the analysis and a total of 250 realizations were executed for each case of analysis. Using Monte Carlo simulation, probabilistic analyses of output parameters were discussed.

The spatial variability of the microscopic friction angle and stiffness leads to smaller mean values of the peak deviator stress $\Delta\sigma_f$ and modulus E_{50} compared to their deterministic values. Increasing the correlation length leads to the positive behavior of the standard deviations of $\Delta\sigma_f$ and E_{50}. The mean values of $\Delta\sigma_f$ and E_{50}, on the other hand, rise from small values of correlation lengths to their peak values at a vertical correlation length θ(y) of about 0.5 m and then falls as θ(y) is greater than 0.5 m.

The algorithm has some advantages in creating 3D discrete element domains accounting for the spatial variability of the properties. The time required to create a 3D soil sample is greatly reduced, 3D random fields of soil properties which are anisotropic and spatially varied can be easily mapped on the soil domain, and the 3D random field generator is embedded into the discrete element code. The proposed algorithm has proved to be efficient and can be implemented to solve other geotechnical problems by coupling reliability analysis and the discrete element method.

ACKNOWLEDGMENT

This research is supported by a research grant from the Natural Sciences and Engineering Research Council of Canada (NSERC). The financial support provided by McGill Engineering Doctoral Award (MEDA) to the first author is greatly appreciated.

REFERENCES

1. Antony SJ, Moreno-Atanasio R, Hassanpour A. Influence of contact stiffnesses on the micromechanical characteristics of dense particulate systems subjected to shearing. *Appl. Phys. Lett* 2006;89, 214 103.
2. Baecher GB, Christian JT. Reliability and statistics in geotechnical engineering. *Wiley, Chichester, U.K* 2003.
3. Belheine N, Plassiard JP, Donze´ FV. Numerical simulation of drained triaxial test using 3D discrete element modeling. *Computers and Geotechnics* 2009; 36:320-331.
4. Christian JT, Baecher GB. Point-estimate method as numerical quadrature. *Journal of Geotechnical and Geoenvironmental Engineering ASCE* 1999; 125(9):779:786.
5. Christian JT, Ladd CC, Baecher GB. Reliability applied to slope stability analysis. *Journal of Geotechnical Engineering ASCE* 1994; 120(2):2180-2207.
6. Cundall P, Strack OD. A discrete numerical model for granular assemblies. *Geotechnique* 1979; 29(1):47-65.
7. Dang HK, Meguid MA. Algorithm to generate a discrete element specimen with predefined properties. *International Journal of Geomechanics* 2010; 10(2):85-91.
8. Deluzarche R, Cambou B. Discrete numerical modeling of rockfill dams. *International Journal for Numerical and Analytical Methods in Geomechanics* 2006; 30:1075–1096.
9. Fenton GA, Griffiths DV. Bearing-capacity prediction of spatially random c – ϕ soil. *Canadian Geotechnical Journal* 2003; 40(1):54-65.
10. Fenton GA, Griffiths DV. Three-Dimensional Probabilistic Foundation Settlement. *J. Geotech. and Geoenvir. Engrg* 2005;131(2):232-239.
11. Fenton GA, Vanmarcke EH. Simulation of Random Fields via Local Average Subdivision. *J. Eng. Mech.* 1990; 116(8):1733-1749.
12. Fu G, Dekelbab W. 3-D random packing of polydisperse particles and concrete aggregate grading. *Powder Technology* 2003; 133(1-3):147-155.
13. Griffiths DV, Fenton GA. Probabilistic Analysis of Exit Gradients due to Steady Seepage. *J. Geotech. and Geoenvir. Engrg* 1998; 124(9):789-797.
14. Griffiths DV, Fenton GA. Probabilistic Settlement Analysis by Stochastic and Random Finite-Element Methods. *J. Geotech. and Geoenvir.. Engrg.* 2009; 135(11):1629-1637.
15. Griffiths DV, Fenton GA. Probabilistic slope stability analysis by finite elements. *J. Geotech. and Geoenvir. Engrg* 2004; 130(5):507-518.
16. Griffiths DV, Fenton GA, Lemons CB. Probabilistic analysis of underground pillar stability. *International Journal for Numerical and Analytical Methods in Geomechanics* 2002; 26:775-791.

17. Hsu SC, Nelson PP. Material spatial variability and slope stability of weak rock masses. *J. Geotech. and Geoenvir. Engrg* 2006; 132(2):183–193.

18. Kozicki J, Donze VF. YADE-OPEN DEM: an open-source software using a discrete element method to simulate granular material. *Engineering Computations* 2009, 26(7):786 – 805.

19. Lobo Guerrero S, Vallejo LE. DEM analysis of crushing around driven piles in granular materials. *Geotechnique* 2005; 55(8):617–623.

20. Low BK, Zhang J, Tang WH. Efficient system reliability analysis illustrated for a retaining wall and a soil slope. *Computers and Geotechnics* 2011, 38(2):196–204.

21. Matthies HG, Brenner CE, Bucher CG, Soares CG. Uncertainties in probabilistic numerical analysis of structures and solids – stochastic finite elements. *Structural Safety* 1997; 19(3):283–336.

22. Melis Maynar MJ, Medina Rodriguez LE. Discrete numerical model for analysis of earth pressure balance tunnel excavation. *Journal of Geotechnical and Geoenvironmental Engineering* 2005; 131(10):1234–1242.

23. Schweiger HF, Peschl GM. Reliability analysis in geotechnics with a random set finite element method. *Computers and Geotechnics* 2005; 32:422–435.

24. Schweiger HF, Thurner R, Pöttler R. Reliability analysis in geotechnics with deterministic finite elements – theoretical concepts and practical application. *Int J Geomech* 2001; 14:389–413.

25. Šmilauer V, Catalano E, Chareyre B, Dorofeenko S, Duriez J, Gladky A, Kozicki J, Modenese C, Scholtès L, Sibille L, Stránský J, Thoeni K. Yade Documentation. The Yade Project 2010. (http://yade-dem.org/doc/).

26. Suchomel R, Mašin D. Comparison of different probabilistic methods for predicting stability of a slope in spatially variable c–φ soil. *Computers and Geotechnics* 2010; 37(1-2):132-140.